

---

---

# Treatment Monitoring by $^{18}\text{F}$ -FDG PET/CT in Patients with Sarcomas: Interobserver Variability of Quantitative Parameters in Treatment-Induced Changes in Histopathologically Responding and Nonresponding Tumors

Matthias R. Benz<sup>1</sup>, Vladimir Evilevitch<sup>1</sup>, Martin S. Allen-Auerbach<sup>1</sup>, Fritz C. Eilber<sup>2</sup>, Michael E. Phelps<sup>1</sup>, Johannes Czernin<sup>1</sup>, and Wolfgang A. Weber<sup>1,3</sup>

<sup>1</sup>Ahmanson Biological Imaging Division, Department of Molecular and Medical Pharmacology, University of California at Los Angeles, Los Angeles, California; <sup>2</sup>Division of Surgical Oncology, Department of Surgery, David Geffen School of Medicine, University of California at Los Angeles, Los Angeles, California; and <sup>3</sup>Abteilung Nuklearmedizin, University of Freiburg, Freiburg, Germany

Measurements of tumor glucose use by  $^{18}\text{F}$ -FDG PET need to be standardized within and across institutions. Various parameters are used for measuring changes in tumor glucose metabolic activity with  $^{18}\text{F}$ -FDG PET in response to cancer treatments. However, it is unknown which of these provide the lowest variability between observers. Knowledge of the interobserver variability of quantitative parameters is important in sarcomas as these tumors are frequently large and demonstrate heterogeneous  $^{18}\text{F}$ -FDG uptake. **Methods:** A total of 33 patients (16 men, 17 women; mean age,  $47 \pm 18$  y) with high-grade sarcomas underwent  $^{18}\text{F}$ -FDG PET/CT scans before and after neoadjuvant chemotherapy. Two independent investigators measured the following parameters on the pretreatment and posttreatment scans: maximum standardized uptake value (SUVmax), peak SUV (SUVpeak), mean SUV (SUVmean), SUVmean in an automatically defined volume (SUVauto), and tumor-to-background ratio (TBR). The variability of the different parameters was compared by concordance correlation coefficient (CCC), variability effect coefficient, and Bland-Altman plots. **Results:** Baseline SUVmax, SUVpeak, SUVmean, SUVauto, and TBR averaged 10.36, 7.78, 4.13, and 6.22 g/mL and 14.67, respectively. They decreased to 5.36, 3.80, 1.79, and 3.25 g/mL and 6.62, respectively, after treatment. SUVmax, SUVpeak, and SUVauto measurements and their changes were reproducible (CCC  $\geq 0.98$ ). However, SUVauto poorly differentiated between responding and nonresponding tumors. The high intratumoral heterogeneity of  $^{18}\text{F}$ -FDG resulted in frequent failure of the thresholding algorithm, which necessitated manual corrections that in turn resulted in a higher interobserver variability of SUVmean (CCCs for follow-up and change were 0.96 and 0.91, respectively;  $P < 0.005$ ). TBRs also showed a sig-

nificantly higher variability than did SUVpeak (CCCs for follow-up and change were 0.94 and 0.86, respectively;  $P < 0.005$ ). **Conclusion:** SUVmax and SUVpeak provided the most robust measurements of tumor glucose metabolism in sarcomas. Delineation of the whole-tumor volume by semiautomatic thresholding did not decrease the variability of SUV measurements. TBRs were significantly more observer-dependent than were absolute SUVs. These findings should be considered for standardization of clinical  $^{18}\text{F}$ -FDG PET/CT trials.

**Key Words:** sarcoma; PET/CT; quantitative analysis; interobserver variability; treatment monitoring

**J Nucl Med 2008; 49:1038–1046**

DOI: 10.2967/jnumed.107.050187

---

**P**ET/CT with the glucose analog  $^{18}\text{F}$ -FDG is increasingly used for monitoring the effectiveness of therapy in patients with malignant diseases (1,2). Use of quantitative measurements of tracer uptake is preferable to use of visual assessment in determining accurately and objectively the degree of tumor response (3,4). Quantitative analysis of tumor  $^{18}\text{F}$ -FDG PET uptake requires delineation of the tumor tissue by regions of interest (ROIs). Various approaches are being used for defining ROIs on  $^{18}\text{F}$ -FDG PET scans including measuring the single maximum pixel value within the slice with the highest radioactivity concentration (maximum standardized uptake value [SUVmax]) (5–7) or placing a fixed ROI in the area of the tumor with the highest level of  $^{18}\text{F}$ -FDG uptake (peak SUV [SUVpeak]) (8–10). Alternatively, volumes of interest (VOIs) can be defined using semiautomated (11–13) or automated (14–16) thresholding algorithms for calculating the mean SUV within this glucose metabolic tumor volume (GMTV) (mean SUV [SUVmean]/mean SUV in an automatically defined volume

Received Dec. 21, 2007; revision accepted Mar. 4, 2008.

For correspondence or reprints contact: Wolfgang Weber, Abteilung Nuklearmedizin, University of Freiburg, Hugstetterstrasse 55, 79106 Freiburg, Germany.

E-mail: wolfgang.weber@uniklinik-freiburg.de

Guest Editor: Barry A. Siegel, Mallinckrodt Institute of Radiology

COPYRIGHT © 2008 by the Society of Nuclear Medicine, Inc.

[SUVauto]). Finally, tumor-to-background ratios (TBRs) have been used frequently for deriving a semiquantitative index of tumor glucose use (3,17).

Most of these different approaches used to define ROIs are not fully automated. Therefore, the interobserver variability of quantitative measurements based on these ROIs must be evaluated. Thus far, however, only limited data on the interobserver variability of ROI definitions are available. Marom et al. (18) used 5 independent readers to determine the SUVmax in 20 patients with non-small-cell lung cancer. SUVmax was determined using 2 different methods: by manually shifting a fixed-size (1-cm) circular ROI around the primary tumor until SUVmax was detected and by creating a freehand drawing around the primary tumor in the slice that visually appeared to exhibit the highest tumor <sup>18</sup>F-FDG uptake. This permitted a comparison between a semiautomated and a manual ROI approach. The SUVmax measurements determined by Marom et al. (18) demonstrated a low variability with Pearson correlation coefficients of more than 0.95 and low variability with several other statistical methods (regression analysis, Bland-Altman analysis, and ANOVA).

Stahl et al. (19) tested the agreement between 2 observers in 40 patients with locally advanced gastric carcinomas and in 10 control subjects; agreement by linear regression analysis was excellent ( $R^2 = 0.97$ ). SUVpeak and SUVmax were derived from manually placed ROIs (diameter, 1.5 cm). Using a similar approach, Avril et al. (20) reported an excellent interobserver variability of SUVpeak between 2 observers in 20 patients with breast cancer.

Knowledge of the interobserver variability of quantitative measurements is becoming increasingly important for the planning of multicenter studies evaluating the usefulness of <sup>18</sup>F-FDG PET for treatment monitoring in larger patient populations. Therefore, we investigated the interobserver variability of commonly used parameters for measuring glucose metabolic activity in patients with sarcomas undergoing <sup>18</sup>F-FDG PET/CT studies before and after neoadjuvant chemotherapy. These parameters included the SUVmax, SUVpeak, SUVmean, SUVauto, and TBRs.

Subsequently, we also determined which parameter of glucose metabolic activity provided the most robust predictions of histopathologic treatment responses. We used sarcomas as the “worst-case scenario” to address the interobserver variability of SUV measurements because of their considerable heterogeneity in <sup>18</sup>F-FDG uptake due to frequently large necrotic areas.

## MATERIALS AND METHODS

### Patients

A total of 33 consecutive patients with biopsy-proven osteosarcoma ( $n = 8$ ) or soft-tissue sarcoma (STS) ( $n = 25$ ) who were considered surgical candidates and were scheduled to undergo operative chemotherapy or chemoradiotherapy were enrolled

prospectively. There were 16 male and 17 female patients (mean age,  $47.1 \pm 17.7$  y; range, 19–86 y).

The most common site of disease was the extremity ( $n = 27$ ; 82%), followed by retroperitoneal or abdominal ( $n = 5$ ; 15%) and chest or trunk ( $n = 1$ ; 3%). Twenty-eight (85%) patients presented with primary disease, 3 (9%) with locally recurrent disease, and 2 (6%) with metastatic disease. Tumors ranged in size from 3.4 to 20.3 cm before treatment and from 2.3 to 25.8 cm after treatment.

All patients underwent a whole-body PET/CT scan before the initiation of neoadjuvant therapy (baseline scan). The baseline PET/CT scan was performed  $8 \pm 6.8$  d before the start of therapy (range, 2–28 d). After the completion of chemotherapy ( $n = 13$ ) or chemoradiotherapy ( $n = 20$ ) and before surgery, patients underwent a second whole-body PET/CT study (follow-up scan).

Tumor resection was performed in all patients after they completed neoadjuvant therapy. Excised tumors were examined for extent of necrosis, and the percentage necrosis was used as the reference standard to assess treatment response. In this study, patients with 10% or fewer viable tumor cells were classified as histopathologic responders as previously described (7).

The study was approved by the UCLA Institutional Review Board for Human Subjects, and written informed consent was obtained from all participants at enrollment.

### PET/CT Image Acquisition and Analysis

Patients were instructed to fast for at least 6 h before <sup>18</sup>F-FDG PET, and blood glucose levels were measured before injection of <sup>18</sup>F-FDG. Patients were excluded if their blood glucose levels at the time of any of the scans exceeded 150 mg/dL (21).

Sixty minutes before the start of imaging, 7.5 MBq of <sup>18</sup>F-FDG per kilogram (0.21 mCi/kg) were injected intravenously.

All patients received 700–900 mL of the oral contrast barium sulfate (Readi-cat 2; EZEM) 1 h before the study. The intravenous contrast iohexol (Omnipaque; Novaplus) was administered in all patients at a rate of 2 mL/s 30–40 s before imaging commenced.

### Image Acquisition

Patients were imaged using a PET/CT system (Biograph Duo; Siemens) consisting of a whole-body PET scanner (ECAT ACCEL; Siemens) and dual-detector helical CT scanner (22). The following parameters were used for CT image acquisition: 130 kVp, 120 mAs, 1-s rotation, 4-mm slice collimation, and 8-mm/s bed speed.

The length of the PET emission scan varied with patient weight as described previously (23). Patients were instructed to use shallow breathing to minimize misregistration and attenuation artifacts between PET and CT images (24).

### PET/CT Image Reconstruction

CT images were reconstructed using conventional filtered back-projection, at 3.4-mm axial intervals to match the slice separation of the PET data. PET images were reconstructed using iterative algorithms (ordered-subset expectation maximization [OSEM], 2 iterations, 8 subsets). To correct for photon attenuation, the previously validated CT-based algorithm was applied (25).

### CT Image Interpretation

A soft-tissue CT window was used to display tumor images on the CT scan. A single observer measured tumor size on the axial slice, with the largest tumor diameter detected on the baseline and the follow-up scans.

## PET Image Interpretation

All PET/CT scans were analyzed quantitatively by 2 independent observers unaware of the clinical data and histopathologic response. Both observers used the same workstation (REVEAL-MVS; CTI Mirada Solutions) to view PET and CT images to define ROIs and VOIs and to coregister baseline and follow-up PET/CT studies. Observers were instructed to use the approaches described in the next sections to place ROIs and VOIs.

### SUVmax

Loosely fitting ROIs covering the whole tumor were placed manually over every axial image plane in which tumor tissue was visualized by abnormal  $^{18}\text{F}$ -FDG accumulation. Then the software determined the SUVmax in this set of ROIs (Fig. 1).

### SUVpeak

The single maximum pixel value within the slice with the highest radioactivity concentration was detected by creating a second circular ROI with a diameter of 15 mm and by moving this ROI over the tumor volume until the single maximum pixel value was detected. Investigators were instructed to place the pixel with the SUVmax at the center of the circular ROI. SUVpeak was defined by the average pixel value within this 15-mm ROI (Fig. 1A). This approach was used for both baseline and follow-up scans.

### SUVauto

SUVauto is the SUVmean of an automatically defined VOI. This VOI includes pixels containing more than 50% of the maximum  $^{18}\text{F}$ -FDG concentration (SUVmax). SUVauto was defined in the baseline and the follow-up scans using the region-growing algorithm implemented in the Mirada software.

### SUVmean

The SUVmean was then determined on baseline and follow-up scans within the tumor borders derived from the baseline PET (Fig. 2). First the baseline GMTV was determined by applying

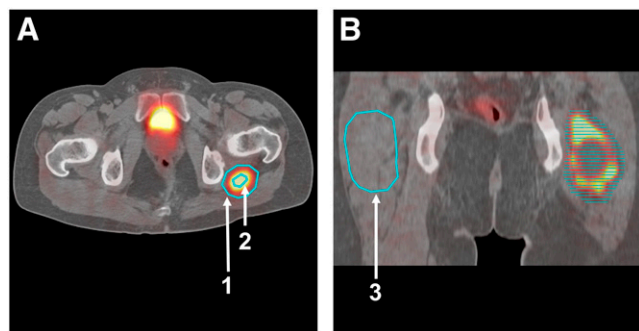


**FIGURE 1.** ROI approach used for detecting SUVmax and SUVpeak within tumor (left thigh) and mean activity concentration in contralateral background region (right thigh). (A) Loosely fitting ROIs were placed manually around entire tumor on every axial image plane in which tumor tissue was visualized by abnormal  $^{18}\text{F}$ -FDG accumulation (arrow 1). (B) All ROIs were placed on multiple axial slices. Each ROI placed on axial images is represented by horizontal line. Within this set of ROIs, computer automatically identified SUVmax. To obtain SUVpeak, 15-mm ROI was manually placed around SUVmax (arrow 2). Then circular ROI was drawn in contralateral normal soft tissue on coronal PET/CT images to determine SUV of background region (arrow 3).

thresholding at 50% of maximum pixel activity as described above.

In some cases normal tissues with relatively high  $^{18}\text{F}$ -FDG uptake were included in the VOIs or the VOIs excluded obvious tumor tissue. In these cases, manual corrections of ROI placement were applied (Fig. 2C).

The GMTV derived from the baseline scan was then copied to the coregistered follow-up study to determine the posttreatment SUVmean. Thus, baseline and follow-up SUVmeans were determined within the same volume.

For coregistration of the baseline and follow-up PET/CT studies, image fusion was performed using the Mirada software. This software is based on a mutual information algorithm as reported previously (26). In this approach, the parameters of transformation are estimated through multidimensional optimization (27). This rigid fusion approach does not use geometric landmarks but searches for feature similarities across voxels instead. The mutual information algorithm was applied to the CT data from the baseline and follow-up scans (Figs. 2D and 2E). This translation information was then used to coregister the baseline and follow-up PET images.

### TBR

Circular ROIs approximately matching the diameter of the tumor were placed in the contralateral normal soft tissue on coronal PET/CT images. The TBR was calculated by dividing the tumor SUVpeak by the mean activity concentration in the contralateral ROI (i.e., the background region) (Fig. 1B).

### Statistical Analysis

Statistical analysis was performed using commercially available software. Values of  $P$  less than 0.05 were considered statistically significant. The absolute values of the measured parameters are expressed as mean  $\pm$  1 SD.

Intra- and interindividual comparisons of absolute values and changes in tumor  $^{18}\text{F}$ -FDG uptake were performed with the Wilcoxon signed rank test and the Mann-Whitney test, respectively. Interobserver variability was assessed by using Lin's concordance correlation coefficient (CCC) (28) and Bland-Altman analysis (29). To determine whether CCCs differed significantly between the various parameters of tumor glucose use, CCCs were compared as reported elsewhere (30). Parameters for assessing the effectiveness of therapy should feature 2 main qualities: low interobserver variability and the ability to differentiate between treatment responders (R) and nonresponders (NR). To combine both qualities in 1 parameter, we defined a variability effect coefficient (VEC) as follows:

$$\frac{|\text{average}(R) - \text{average}(NR)|}{\sqrt{[\text{SD}(R)]^2 + [\text{SD}(NR)]^2}} \bigg/ 1 + \frac{\text{SD}(\text{OB})}{\sqrt{[\text{SD}(R)]^2 + [\text{SD}(NR)]^2}}$$

where average(R) and average(NR) denote the mean value of a parameter for the group of histopathologic responders and nonresponders, respectively, and SD(R) and SD(NR) represent the SD of a parameter in the responders and nonresponders, respectively. For calculation of average(R), average(NR), SD(R), and SD(NR), the measurements of observer 1 and observer 2 were averaged for each tumor. For calculation of SD(OB), the SDs of the measurements of the 2 observers were determined for each tumor and the resulting 33 SDs were averaged.

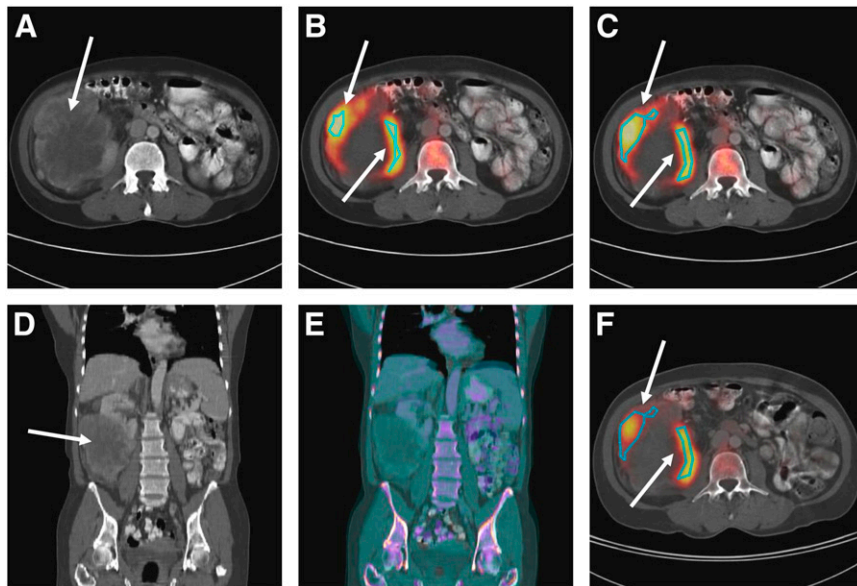


**FIGURE 2.** (A) Dedifferentiated liposarcoma located in right lower abdomen (arrows). (B) For placement of ROI, 50% isocontour thresholding approach was used. (C) ROI from B was manually adjusted to better fit hypermetabolic region. (D) Tumor in coronal views. To ascertain identical ROI placement in baseline and follow-up studies, 2 CT images were fused (E). Baseline images in D are displayed in gray scale, whereas follow-up images are color-scaled. (F) ROI placement used in follow-up was identical to that used in baseline scan in C.

Thus, the enumerator of the VEC describes how well a parameter separates the histopathologic responders from the nonresponders, that is, by how many SDs the parameter differs in responders and nonresponders. The denominator of the VEC describes the interobserver variability of the measurements. When no interobserver variability exists, the denominator becomes 1. A high VEC therefore indicates that a parameter shows a low interobserver variability and separates well the histopathologic responders from the nonresponders.

## RESULTS

### Histopathology

On the basis of excised tumor tissue, 10 patients were classified as histopathologic responders ( $\geq 90\%$  necrosis) and 23 as nonresponders (30.3% response rate). The average percentage of tumor necrosis was 65%, ranging from 9% to 99.9%. Thus, tumors exhibited high inter- and intratumoral heterogeneity in  $^{18}\text{F}$ -FDG-uptake at baseline and at follow-up (Table 1).

### SUV and TBR Measurements

Baseline and follow-up  $^{18}\text{F}$ -FDG uptake parameters as determined by the 2 observers are listed in Table 1. SUVmax, SUVpeak, SUVmean, SUVauto, and TBR averaged 10.36, 7.78, 4.13, and 6.22 g/mL and 14.67, respectively, at baseline. They decreased to 5.36, 3.80, 1.79, and 3.25 g/mL and 6.62, respectively, after treatment (all  $P < 0.005$ ).

The data were further stratified by histopathologic response (Fig. 3). Changes in SUVmax, SUVpeak, and SUVmean were significantly more pronounced in responders than in nonresponders ( $P < 0.005$ ).

In the baseline scans, SUVmax and SUVauto measurements of the 2 readers were identical in all studies (100% concordance, CCC = 1), indicating that the procedure for

observer-independent identification of maximum tumor  $^{18}\text{F}$ -FDG uptake was successful in all cases. SUVpeak also demonstrated a low interobserver variability (CCC = 0.99), and interobserver variability was significantly higher for SUVmean and TBR (CCC = 0.84 and CCC = 0.92, respectively;  $P < 0.005$ ).

An identical ranking of the CCC was found for the follow-up study and for changes from the baseline to the follow-up study. (SUVmax = SUVauto > SUVpeak > SUVmean > TBR). Again, SUVmean and TBR demonstrated a higher interobserver variability than did SUVmax, SUVpeak, and SUVauto (Table 2).

SUVpeak, SUVmean, and TBR changes from the baseline to follow-up scan tended to show a higher interobserver variability than did the pretherapeutic or posttherapeutic SUVpeak, SUVmean, or TBR measurements (Table 2).

The Bland-Altman plots in Figure 4 illustrate the higher interobserver variability of SUVmean and TBR than of SUVpeak for SUV and TBR changes. Bland-Altman plots for baseline and posttherapeutic SUV also indicated a lower interobserver variability of SUVpeak than of SUVmean and TBR (data not shown). The SD of differences of measurements by observer 1 and observer 2 is shown in Table 2. This type of analysis also ranked the interobserver variability of SUVpeak lower than that of SUVmean and TBR (Table 2).

The VEC that combines interobserver variability and the ability to differentiate between treatment responders and nonresponders was higher for changes in SUV than for absolute SUVs or TBRs. Among the changes in parameters, the VEC ranking was as follows: SUVmax > SUVpeak > SUVmean > TBR > SUVauto (Fig. 5). Thus, SUVauto was a relatively poor parameter to differentiate histopathologic responders and nonresponders, despite its excellent interobserver variability.

**TABLE 1**  
SUV Parameters and Their Changes as Assessed by 2 Observers

Parameter	Baseline				Follow-up				% reduction			
	All patients		Nonresponders		All patients		Nonresponders		All patients		Nonresponders	
	Mean	Range	Mean	Range	Mean	Range	Mean	Range	Mean	Range	Mean	Range
<b>SUVmax</b>												
Mean	10.36 ± 7.68	12.68 ± 8.30	9.35 ± 7.36	5.36 ± 4.54	3.27 ± 1.60	6.26 ± 5.10	67 ± 17	29 ± 35				
Range	2.48-29.91	3.63-29.91	2.48-29.47	1.24-22.45	1.77-6.85	1.24-22.45	38-88	-73-69				
Observer 1	10.36 ± 7.68	12.68 ± 8.30	9.35 ± 7.36	5.36 ± 4.54	3.27 ± 1.60	6.26 ± 5.10	67 ± 17	29 ± 35				
Range	2.48-29.91	3.63-29.91	2.48-29.47	1.24-22.45	1.77-6.85	1.24-22.45	38-88	-73-69				
Observer 2	10.36 ± 7.68	12.68 ± 8.30	9.35 ± 7.36	5.36 ± 4.54	3.27 ± 1.60	6.26 ± 5.10	67 ± 17	29 ± 35				
Range	2.48-29.91	3.63-29.91	2.48-29.47	1.24-22.45	1.77-6.85	1.24-22.45	38-88	-73-69				
<b>SUVpeak</b>												
Mean	7.78 ± 5.69	9.50 ± 6.69	7.03 ± 5.19	3.80 ± 3.08	2.37 ± 1.01	4.42 ± 3.47	67 ± 16	32 ± 33				
Range	2.09-23.88	2.76-23.88	2.09-20.55	0.94-16.77	1.41-4.63	0.94-16.77	38-88	-57-69				
Observer 1	7.73 ± 5.74	9.34 ± 6.91	7.03 ± 5.16	3.78 ± 3.07	2.32 ± 1.00	4.42 ± 3.45	67 ± 16	32 ± 32				
Range	2.08-24.41	2.71-24.41	2.08-20.49	0.88-16.60	1.38-4.55	0.88-16.60	41-87	-48-69				
Observer 2	7.82 ± 5.67	9.66 ± 6.51	7.02 ± 5.22	3.82 ± 3.10	2.42 ± 1.03	4.43 ± 3.50	68 ± 16	32 ± 33				
Range	2.09-23.35	2.81-23.35	2.09-20.61	1.00-16.94	1.44-4.71	1.00-16.94	36-89	-65-69				
<b>SUVmean</b>												
Mean	4.13 ± 2.44	4.58 ± 2.37	3.94 ± 2.50	1.79 ± 1.13	1.15 ± 0.40	2.07 ± 1.24	70 ± 13	41 ± 27				
Range	1.31-10.99	1.31-8.27	1.41-10.99	0.48-5.20	0.48-1.92	0.48-5.20	47-87	-40-88				
Observer 1	4.05 ± 2.33	4.55 ± 2.36	3.83 ± 2.33	1.82 ± 1.21	1.12 ± 0.42	2.12 ± 1.32	70 ± 14	40 ± 30				
Range	1.30-11.94	1.30-7.73	1.37-11.94	0.49-5.42	0.49-1.95	0.50-5.42	45-88	-58-89				
Observer 2	4.22 ± 2.74	4.61 ± 2.43	4.05 ± 2.90	1.77 ± 1.08	1.18 ± 0.38	2.03 ± 1.19	70 ± 12	43 ± 25				
Range	1.32-14.33	1.32-8.81	1.37-14.33	0.46-4.98	0.47-1.89	0.46-4.98	49-86	-21-87				
<b>TBR</b>												
Mean	14.67 ± 11.78	18.34 ± 13.43	13.08 ± 10.92	6.62 ± 6.01	3.67 ± 1.69	7.89 ± 6.77	73 ± 15	31 ± 41				
Range	2.23-45.89	5.29-44.06	2.23-45.89	1.76-26.83	1.76-7.47	2.01-26.83	43-94	-81-79				
Observer 1	15.06 ± 13.18	19.24 ± 15.18	13.25 ± 12.12	6.67 ± 6.10	3.65 ± 1.63	7.99 ± 6.86	73 ± 15	29 ± 43				
Range	2.04-55.89	6.45-47.86	2.04-55.89	1.45-26.77	1.45-7.22	1.70-26.77	46-95	-93-80				
Observer 2	14.28 ± 10.75	17.44 ± 11.97	12.91 ± 10.15	6.56 ± 6.11	3.70 ± 1.81	7.80 ± 6.91	72 ± 16	33 ± 42				
Range	2.43-42.06	4.13-40.26	2.43-42.06	2.08-26.89	2.08-7.72	2.11-26.89	40-93	-87-81				
<b>SUVbg</b>												
Mean	0.59 ± 0.20	0.58 ± 0.28	0.59 ± 0.16	0.65 ± 0.23	0.70 ± 0.32	0.63 ± 0.19	-30 ± 39	-12 ± 35				
Range	0.30-1.28	0.30-1.28	0.33-1.05	0.39-1.55	0.42-1.55	0.39-1.13	-102-0	-118-34				
Observer 1	0.59 ± 0.24	0.54 ± 0.29	0.60 ± 0.21	0.66 ± 0.30	0.71 ± 0.41	0.63 ± 0.25	-86	-11 ± 47				
Range	0.25-1.26	0.25-1.26	0.30-1.18	0.28-1.81	0.34-1.81	0.28-1.21	-148-4	-173-42				
Observer 2	0.59 ± 0.18	0.61 ± 0.27	0.58 ± 0.13	0.65 ± 0.19	0.69 ± 0.24	0.63 ± 0.16	-57	-13 ± 31				
Range	0.28-1.29	0.28-1.29	0.32-0.91	0.35-1.28	0.49-1.28	0.35-1.04	-104-14	-88-31				

SUVbg = SUV of background region.

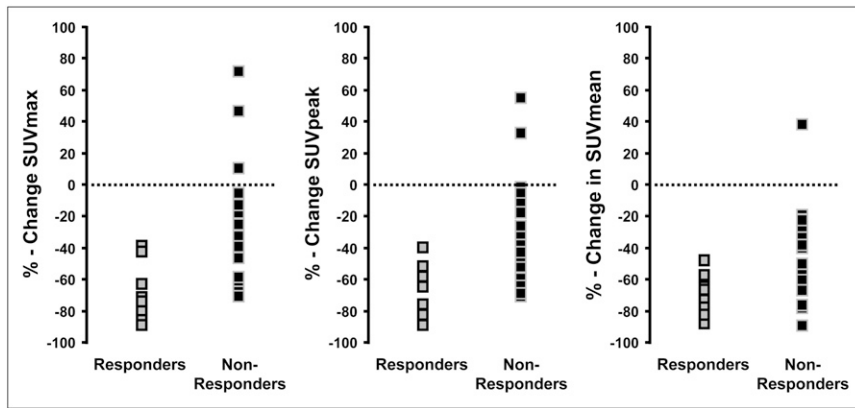


**FIGURE 3.** Changes in tumor SUVmax, SUVpeak, and SUVmean are stratified for responders and nonresponders as defined by histopathology. Each data point represents mean of measurements of 2 observers.

## DISCUSSION

The present study indicates that different approaches to define ROIs result in considerably different interobserver variability. Specifically, SUVmean and TBR demonstrated a significantly higher interobserver variability than did SUVmax, SUVpeak, and SUVauto. Although this seems to suggest that the latter parameters are preferable to SUVmean and TBR for treatment monitoring, our study also indicates that focusing on the interobserver variability alone can be misleading. An automated thresholding approach for delineation of tumor contours (SUVauto) provided observer-independent results but was a poor discriminator between histopathologically responding and nonresponding tumors.

**TABLE 2**

CCC, SD of Differences, and Comparison Between CCCs

Parameter	CCC	Lower 95% CI for CCC	SD of differences	P (comparing 2 CCCs)
<b>Baseline</b>				
SUVmax	1.00	1.00	0.00	
SUVpeak	0.99	0.99	0.68	<0.005*
SUVmean	0.84	0.71	1.42	<0.005†
SUVauto	1.00	1.00	0.00	
TBR	0.92	0.85	4.86	NS‡
<b>Follow-up</b>				
SUVmax	1.00	1.00	0.00	
SUVpeak	0.99	0.99	0.20	<0.005*
SUVmean	0.96	0.92	0.33	<0.005†
SUVauto	1.00	1.00	0.00	
TBR	0.94	0.88	2.10	NS‡
<b>Change</b>				
SUVmax	1.00	1.00	0	
SUVpeak	0.98	0.96	6%	<0.005*
SUVmean	0.91	0.83	11%	<0.005†
SUVauto	1.00	1.00	0	
TBR	0.86	0.74	21%	NS‡

\*SUVpeak vs. SUVmean.

†SUVpeak vs. TBR.

‡SUVmean vs. TBR.

CI = confidence interval; NS = not significant.

We therefore propose that the interobserver variability of parameters for monitoring the effects of cancer therapy should be measured on the basis of their ability to differentiate responding and nonresponding tumors. When applying such a metric, the most suitable parameters for monitoring tumor response in patients with STSs were SUVmax and SUVpeak. Our findings confirm that in patients with sarcoma, SUVmax and SUVpeak provide reproducible parameters of tumor glucose use (19,20). However, the excellent interobserver variability of SUVmax can be achieved only when observers are provided with an accurate guideline for detecting SUVmax. Furthermore, the use of combined PET/CT facilitated ROI placement in the appropriate anatomic location (31).

In contrast, mean SUV and TBR measurements were associated with considerable variability. This observation is consistent with results from a previous study by Hashimoto et al. (32). In that study, 43 patients with benign and malignant solid pulmonary lesions with <sup>18</sup>F-FDG SUVs less than 2.5 were semiquantitatively analyzed by 2 independent raters. The interobserver concordance of SUVmax and SUVmax-to-background ratios was tested using the coefficient of variation. TBRs were determined by measuring the highest activity in the tumor ROI (SUVmax) and in the contralateral normal lung ROI (background). The introduction of a background ROI resulted in a high variability of quantitative measurements (coefficient of variation, 142%), which agreed with our results. The relatively high interobserver variability of TBR relates to the calculation of a TBR requiring the definition of a second ROI, which introduces another observer-dependent factor. Furthermore, counting rates in normal lung tissue are low. This makes a TBR in the lung very sensitive to image noise.

To minimize interobserver variability and the effect of image noise, we instructed observers to draw large background lesions for assessing TBRs. Nevertheless, they showed low concordance, which was primarily because of a high interobserver variability in SUVs from background regions.

The high interobserver variability of SUVmean may appear surprising, because SUVmax measurements were

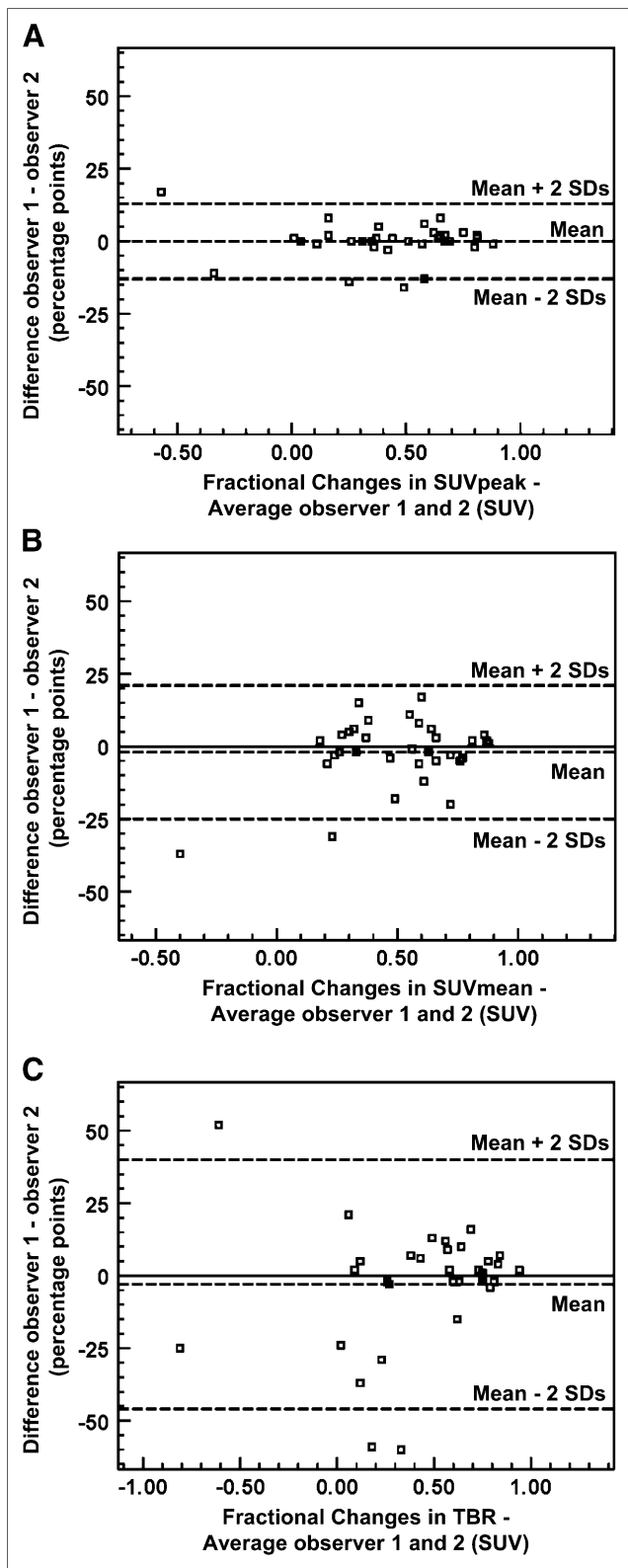


**FIGURE 4.** Bland-Altman plots exemplifying that differences between observers 1 and 2 were smaller for changes in SUVpeak (A) than for changes in SUVmean (B) and in TBR (C).

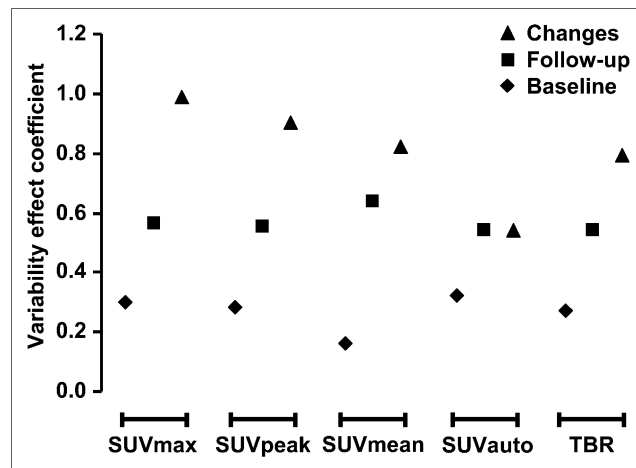


**FIGURE 5.** VEC combining interobserver variability and ability to differentiate between treatment responders and nonresponders. High coefficient signifies robust and valid data. VEC was higher for changes in SUV than for absolute SUVs or TBR. Changes in parameters rather than their absolute values are preferable for assessing effectiveness of therapy.

100% concordant between the 2 investigators, and the ROI for calculation of SUVmean was defined to include all adjacent pixels with  $^{18}\text{F}$ -FDG-uptake of at least 50% of the maximum. However, in all 33 cases manual corrections were performed eventually, because the tumor contours based on a single threshold value excluded obvious tumor tissue or included adjacent normal tissue (Fig. 2). We tried to minimize the effect of interobserver variability by defining the tumor contours only in the baseline study and then reorienting the follow-up scan to the baseline study by a mutual information algorithm. Nevertheless, the manual adjustments of the ROIs introduced a relatively high degree of interobserver variability.

When no manual adjustments were performed, interobserver variability was eliminated, but the resulting parameter, SUVauto, poorly differentiated between responding and nonresponding tumors. The poor performance of SUVauto was because inhomogeneous  $^{18}\text{F}$ -FDG uptake frequently caused the automatically defined tumor contours to include large areas of normal tissues (Fig. 6) or excluded large parts of the tumor mass (Fig. 2). However, STSs demonstrate a particularly high inter- and intratumoral heterogeneity of  $^{18}\text{F}$ -FDG uptake. In tumors with more homogeneous  $^{18}\text{F}$ -FDG uptake, a thresholding approach may be more appropriate.

In this study, we used several commonly applied approaches (CCC, Bland-Altman plots) to assess the interobserver variability of different approaches for ROI definition. All these established approaches ranked the interobserver variability of the tested parameters in the same order (SUVmax = SUVauto < SUVpeak < SUVmean < TBR). However, a low interobserver variability is only 1 parameter for reliably assessing tumor responses to therapy; it is also important that the differences between

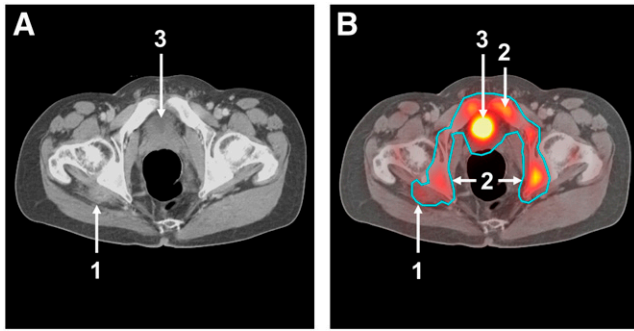


**FIGURE 6.** Images depicting treated, histopathologically responding malignant peripheral nerve sheath tumor located in right gluteal area. (A) Tumor on axial CT soft-tissue window (arrow 1). (B) ROI placement using 50% isocontour thresholding approach. This automatically defined contour includes tumor (arrow 1) and large area of normal tissues (bone marrow, arrow 2; bladder, arrow 3).

responding and nonresponding tumors are compared with the interobserver variability. Therefore, we introduced the VEC and determined the ability of all tested parameters to differentiate between histopathologic responders and nonresponders (Fig. 5).

In this approach, low variability between observers (denominator) and large differences in parameters between histopathologic responders and nonresponders (numerator) resulted in a high coefficient signifying robust and valid data. Changes in SUV parameters tend to show higher interobserver variability (as indicated by lower CCCs). Nevertheless, the introduction of the VEC supports the notion that changes in these parameters rather than their absolute values are preferable for assessing the effectiveness of therapy (Fig. 5).

SUVmax showed the highest VEC, indicating low interobserver variability and good separation between responding and nonresponding tumors. However, SUVmax and to a lesser extent also SUVpeak are more prone to variations due to statistical noise as well as image reconstruction and parameters after processing (33). Therefore, the use of SUVmax might be limited when studies are performed on different PET scanners as can be the case in multicenter clinical trials.

The following proved to be limitations of this study. First, we analyzed the interobserver variability of 5 commonly used approaches to quantify tumor  $^{18}\text{F}$ -FDG uptake. However, several other and more sophisticated techniques have been described that may provide a better segmentation of the tumor tissue. These include, among others, the use of higher threshold values (e.g., 70%) for tumor segmentation (34–36), correction of background activity before segmentation (11,12), and isocontour methods that take into account local contrast (37,38). An analysis of the interobserver variability of all these approaches for tumor segmentation is beyond the scope of this investigation and warrants future studies. Second, images were reconstructed

with 1 set of parameters routinely used for clinical PET/CT scans. However, other reconstruction parameters may facilitate tumor delineation by thresholding techniques. For example, less smoothing during reconstruction may facilitate delineation of tumors with a 50% isocontour, because image contrast is increased. Future studies are needed to systematically evaluate the impact of image reconstruction and postprocessing on interobserver variability and on the ability of quantitative parameters to separate histopathologically responding from nonresponding tumors.

## CONCLUSION

We have expanded on previous studies by systematically testing several frequently used parameters for estimating tumor glucose use. SUVmax and SUVpeak showed low variability and effectively separated histopathologically responding and nonresponding tumors. TBRs and SUVmean were significantly more observer-dependent than were SUVpeak and SUVmax. An automated delineation of tumor borders by a thresholding algorithm provided reproducible results but failed to correctly delineate tumor borders. As a consequence, this approach was not useful for differentiating histopathologically responding and nonresponding tumors. Further studies will have to elucidate whether these findings obtained in glucose metabolically heterogeneous sarcomas can be reproduced in smaller lesions and tumor types with less heterogeneous  $^{18}\text{F}$ -FDG uptake.

## REFERENCES

- Juwaid ME, Cheson BD. Positron-emission tomography and assessment of cancer therapy. *N Engl J Med.* 2006;354:496–507.
- Weber WA, Figlin R. Monitoring cancer treatment with PET/CT: does it make a difference? *J Nucl Med.* 2007;48(suppl):36S–44S.
- Lin C, Itti E, Haioun C, et al. Early  $^{18}\text{F}$ -FDG PET for prediction of prognosis in patients with diffuse large B-cell lymphoma: SUV-based assessment versus visual analysis. *J Nucl Med.* 2007;48:1626–1632.
- Weber WA, Wieder H. Monitoring chemotherapy and radiotherapy of solid tumors. *Eur J Nucl Med Mol Imaging.* 2006;33(suppl 1):27–37.
- Rousseau C, Devillers A, Sagan C, et al. Monitoring of early response to neoadjuvant chemotherapy in stage II and III breast cancer by [ $^{18}\text{F}$ ]fluorodeoxyglucose positron emission tomography. *J Clin Oncol.* 2006;24:5366–5372.
- Schelling M, Avril N, Nahrig J, et al. Positron emission tomography using [ $^{18}\text{F}$ ]fluorodeoxyglucose for monitoring primary chemotherapy in breast cancer. *J Clin Oncol.* 2000;18:1689–1695.
- Schuetz SM, Rubin BP, Vernon C, et al. Use of positron emission tomography in localized extremity soft tissue sarcoma treated with neoadjuvant chemotherapy. *Cancer.* 2005;103:339–348.
- Ott K, Fink U, Becker K, et al. Prediction of response to preoperative chemotherapy in gastric carcinoma by metabolic imaging: results of a prospective trial. *J Clin Oncol.* 2003;21:4604–4610.
- Avril N, Sassen S, Schmalfeldt B, et al. Prediction of response to neoadjuvant chemotherapy by sequential F-18-fluorodeoxyglucose positron emission tomography in patients with advanced-stage ovarian cancer. *J Clin Oncol.* 2005;23:7445–7453.
- Weber WA, Ott K, Becker K, et al. Prediction of response to preoperative chemotherapy in adenocarcinomas of the esophagogastric junction by metabolic imaging. *J Clin Oncol.* 2001;19:3058–3065.
- Eschmann SM, Friedel G, Paulsen F, et al.  $^{18}\text{F}$ -FDG PET for assessment of therapy response and preoperative re-evaluation after neoadjuvant radio-chemotherapy in stage III non-small cell lung cancer. *Eur J Nucl Med Mol Imaging.* 2007;34:463–471.



12. Hoekstra CJ, Stroobants SG, Smit EF, et al. Prognostic relevance of response evaluation using [<sup>18</sup>F]-2-fluoro-2-deoxy-D-glucose positron emission tomography in patients with locally advanced non-small-cell lung cancer. *J Clin Oncol*. 2005;23:8362–8370.
13. Cascini GL, Avallone A, Delrio P, et al. <sup>18</sup>F-FDG PET is an early predictor of pathologic tumor response to preoperative radiochemotherapy in locally advanced rectal cancer. *J Nucl Med*. 2006;47:1241–1248.
14. Weber WA, Ziegler SI, Thodtmann R, Hanauske AR, Schwaiger M. Reproducibility of metabolic measurements in malignant tumors using FDG PET. *J Nucl Med*. 1999;40:1771–1777.
15. Scarfone C, Lavelly WC, Cmelak AJ, et al. Prospective feasibility trial of radiotherapy target definition for head and neck cancer using 3-dimensional PET and CT imaging. *J Nucl Med*. 2004;45:543–552.
16. Mah K, Caldwell CB, Ung YC, et al. The impact of <sup>18</sup>F-FDG-PET on target and critical organs in CT-based treatment planning of patients with poorly defined non-small-cell lung carcinoma: a prospective study. *Int J Radiat Oncol Biol Phys*. 2002;52:339–350.
17. Weber WA, Petersen V, Schmidt B, et al. Positron emission tomography in non-small-cell lung cancer: prediction of response to chemotherapy by quantitative assessment of glucose use. *J Clin Oncol*. 2003;21:2651–2657.
18. Marom EM, Munden RF, Truong MT, et al. Interobserver and intraobserver variability of standardized uptake value measurements in non-small-cell lung cancer. *J Thorac Imaging*. 2006;21:205–212.
19. Stahl A, Ott K, Weber WA, et al. FDG PET imaging of locally advanced gastric carcinomas: correlation with endoscopic and histopathological findings. *Eur J Nucl Med Mol Imaging*. 2003;30:288–295.
20. Avril N, Bense S, Ziegler SI, et al. Breast imaging with fluorine-18-FDG PET: quantitative image analysis. *J Nucl Med*. 1997;38:1186–1191.
21. Shankar LK, Hoffman JM, Bacharach S, et al. Consensus recommendations for the use of <sup>18</sup>F-FDG PET as an indicator of therapeutic response in patients in National Cancer Institute trials. *J Nucl Med*. 2006;47:1059–1066.
22. Allen-Auerbach M, Yeom K, Park J, Phelps M, Czernin J. Standard PET/CT of the chest during shallow breathing is inadequate for comprehensive staging of lung cancer. *J Nucl Med*. 2006;47:298–301.
23. Halpern BS, Dahlbom M, Quon A, et al. Impact of patient weight and emission scan duration on PET/CT image quality and lesion detectability. *J Nucl Med*. 2004;45:797–801.
24. Goerres GW, Burger C, Kamel E, et al. Respiration-induced attenuation artifact at PET/CT: technical considerations. *Radiology*. 2003;226:906–910.
25. Kinahan PE, Townsend DW, Beyer T, Sashin D. Attenuation correction for a combined 3D PET/CT scanner. *Med Phys*. 1998;25:2046–2053.
26. Roche A, Malandain G, Ayache N. Unifying maximum likelihood approaches in medical image registration. *Int J Imaging Syst Technol*. 2000;11:71–80.
27. Rueckert D, Hayes C, Stodholme C, Summers P, Leach M, Hawkes D. Non-rigid registration of breast MR images using mutual information. *Lecture Notes Comput Sci*. 1998;1496:1144–1152.
28. Lin LI. A concordance correlation coefficient to evaluate reproducibility. *Biometrics*. 1989;45:255–268.
29. Bland JM, Altman DG. Statistical methods for assessing agreement between two methods of clinical measurement. *Lancet*. 1986;1:307–310.
30. Zar JH. *Biostatistical Analysis*. Upper Saddle River, NJ: Prentice Hall; 1999.
31. Syed R, Bomanji JB, Nagabhushan N, et al. Impact of combined <sup>18</sup>F-FDG PET/CT in head and neck tumours. *Br J Cancer*. 2005;92:1046–1050.
32. Hashimoto Y, Tsujikawa T, Kondo C, et al. Accuracy of PET for diagnosis of solid pulmonary lesions with <sup>18</sup>F-FDG uptake below the standardized uptake value of 2.5. *J Nucl Med*. 2006;47:426–431.
33. Boellaard R, Krak NC, Hoekstra OS, Lammertsma AA. Effects of noise, image resolution, and ROI definition on the accuracy of standard uptake values: a simulation study. *J Nucl Med*. 2004;45:1519–1527.
34. Graham MM, Peterson LM, Hayward RM. Comparison of simplified quantitative analyses of FDG uptake. *Nucl Med Biol*. 2000;27:647–655.
35. Hunter GJ, Hamberg LM, Alpert NM, Choi NC, Fischman AJ. Simplified measurement of deoxyglucose utilization rate. *J Nucl Med*. 1996;37:950–955.
36. Lee JR, Madsen MT, Bushnell D, Menda Y. A threshold method to improve standardized uptake value reproducibility. *Nucl Med Commun*. 2000;21:685–690.
37. van Dalen JA, Hoffmann AL, Dicken V, et al. A novel iterative method for lesion delineation and volumetric quantification with FDG PET. *Nucl Med Commun*. 2007;28:485–493.
38. Daisne JF, Sibomana M, Bol A, Doumont T, Lonnet M, Gregoire V. Tridimensional automatic segmentation of PET volumes based on measured source-to-background ratios: influence of reconstruction algorithms. *Radiother Oncol*. 2003;69:247–250.